ELSEVIER

Journal of Electron Spectroscopy and Related Phenomena 98–99 (1999) 1–15

JOURNAL OF ELECTRON SPECTROSCOPY and Related Phenomena

Surface sensitivity of Auger-electron spectroscopy and X-ray photoelectron spectroscopy

C.J. Powell[a,*], A. Jablonski[b], I.S. Tilinin[c], S. Tanuma[d], D. R. Penn[e]

[a]*Surface and Microanalysis Science Division, National Institute of Standards and Technology, Gaithersburg, MD 20899, USA*
[b]*Institute of Physical Chemistry, Polish Academy of Sciences, ul. Kasprzaka 44/52, 01-224 Warsaw, Poland*
[c]*Materials Science Division, Lawrence Berkeley National Laboratory, 1 Cyclotron Road, Berkeley, CA 94720, USA*
[d]*Japan Energy ARC Co. Ltd., 3-17-35 Niizo-Minami, Toda-shi, Saitama 335, Japan*
[e]*Electron and Optical Physics Division, National Institute of Standards and Technology, Gaithersburg, MD 20899, USA*

Accepted 17 February 1998

Abstract

A convenient measure of surface sensitivity in Auger-electron spectroscopy (AES) and X-ray photoelectron spectroscopy (XPS) is the mean escape depth (MED). If the effects of elastic-electron scattering are neglected, the MED is equal to the electron inelastic mean free path (IMFP) multiplied by the cosine of the emission angle with respect to the surface normal, and depends on the material and electron energy of interest. An overview is given here of recent calculations of IMFPs for 50–2000 eV electrons in a range of materials. This work has led to the development of a predictive formula based on the Bethe equation for inelastic electron scattering in matter from which IMFPs can be determined. Estimates show, however, that elastic-electron scattering can significantly modify the MED. Thus, for AES, the MED will be reduced by up to about 35%. For XPS, however, the MED can be changed by up to ± 30% for common measurement conditions although it can be much larger (by up to a factor of 2) for near-grazing emission angles. Ratios of MED values, calculated with elastic scattering considered and neglected for XPS from the 3s, 3p, and 3d subshells of silver with Mg Kα X-rays are approximately constant (to about 10%) over a range of emission angles that varies from 40° to 60° depending on the subshell and the angle of X-ray incidence. Recommendations are given on how to determine the optimum range of emission angles for satisfactory analysis of angle-resolved XPS (ARXPS) data. Definitions are included of three terms often used for describing surface sensitivity (IMFP, MED, and effective attenuation length (EAL)), and examples are given of the varying magnitudes of these quantities for different analytical conditions.

Keywords: Auger-electron spectroscopy; X-ray photoelectron spectroscopy; Surface sensitivity; Elastic-electron scattering; Inelastic-electron scattering

1. Introduction

Auger-electron spectroscopy (AES) and X-ray photoelectron spectroscopy (XPS) have developed rapidly since commercial instruments became available about thirty years ago [1]. These techniques are now used extensively in many different areas of science and technology. For XPS alone, a recent computer-aided literature search revealed that approximately 2000 papers were being published each year in over 400 journals.

An important objective in the early days of AES and XPS was to determine the surface sensitivity of these techniques. For this purpose, many experiments

* Corresponding author.

0368-2048/99/$ - see front matter
PII: S0368-2048(98)00271-0

were performed to measure changes of signal intensities as films of one material were deposited on another. Dick Brundle was the author of one of three review articles published in 1974 [2–4] that reviewed the state of knowledge in this field at the time. One important benefit of the Brundle review was to dispel the notion that had arisen suggesting that the surface sensitivity of Auger electrons in a material might be different from that of photoelectrons of the same energy. The three 1974 reviews were largely superseded by a 1979 compilation of similar data by Seah and Dench [5]. It was not until the 1980s, however, with the advent of scanning tunneling microscopy, that atomic-scale measurements could be readily made of the structure and morphology of growing films. These experiments led to the realization that data from the earlier overlayer experiments should be regarded as, at best, a semi-quantitative guide because the overlayer films were unlikely to be of uniform thickness, as assumed in the analysis [6]. Indeed, the extreme values of replicate measurements in eight laboratories of effective attenuation lengths (see Appendix for definition) for photoelectrons excited from the silicon 2p shell by aluminum and magnesium characteristic X-rays differed by a factor of up to three [7]. While it might be tempting to consider the extreme values as "outliers," there is no known justification for this assumption.

One result of the initial attempts to determine surface sensitivity in AES and XPS was the development of a concept known as the "universal curve." The early measurements of effective attenuation lengths (EALs) for different solid elements did not show an appreciable material dependence [2–4] although, as we know now, the uncertainties in the EAL measurements were considerable. The available measurements tended to cluster about a common curve when the EALs were plotted against electron energy on logarithmic scales, and this curve was referred to as the universal curve. Specific curves of this type were later developed for groups of elements, inorganic compounds, and organic compounds [5]. The universal curve concept was indeed helpful in providing a general orientation to students or to new users of AES and XPS and was also very useful in early determinations of surface composition by AES and XPS. Nevertheless, there can be appreciable variations in the inelastic mean free paths (see Appendix for definition) for different materials (at the same electron energy) and in the dependence of the inelastic mean free path on energy for different materials [8,9]. It is therefore disappointing to find early examples of the "universal curve" still appearing in a recent text [10].

Three terms, the inelastic mean free path (IMFP), the effective attenuation length (EAL), and the mean escape depth (MED), have been used in different contexts to give a measure of the surface sensitivity of AES and XPS. Since these terms are often used incorrectly (many authors regard the terms as interchangeable), we give their definitions in the Appendix. In this article, the MED will be used as the measure of surface sensitivity since comparisons can be easily made of values determined with and without consideration of the effects of elastic-electron scattering.

If the effects of elastic-electron scattering in the specimen material are ignored, the MED of the detected electrons in AES and XPS is given simply by

$$\Delta = \lambda \cos\alpha \qquad (1)$$

where λ is the IMFP and α is the electron emission angle with respect to the surface normal. This simple relation is the basis of much recent work [11,12] to obtain composition-versus-depth information using angle-resolved XPS (ARXPS) and AES. It has now been established, however, that elastic-electron scattering can appreciably modify the contributions to the signal arising from different depths (the depth distribution function) and thus the MED [13–15] This effect is particularly pronounced for XPS since the photoionization process is anisotropic. As a result, the XPS signal intensity in certain emission directions can be appreciably enhanced or reduced due to elastic-scattering effects.

In this article we give an overview of recent work to evaluate the MED for AES and XPS. In Section 2, we describe recent calculations of IMFPs and the development of a predictive IMFP formula [16–21]. We then show the magnitude of elastic-scattering effects on the MED for XPS [22–24] and AES [25–28] in Section 3. Specific guidance is given on the selection of an appropriate range of emission angles for reliable analysis of ARXPS data. Atomic elastic-scattering cross sections have been used here, and the results

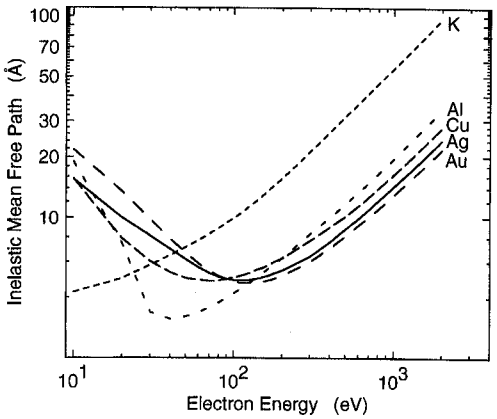

Fig. 1. IMFPs calculated for Al, Cu, Ag, Au [16–21] and K [34] as a function of electron energy. The IMFPs shown for 10–40 eV electrons illustrate trends but are not considered reliable because the Penn algorithm [29] is not valid for such low energies [16–21].

are thus applicable only to amorphous or polycrystalline solids. A summary is given in Section 4.

2. Calculations of inelastic mean free paths

Tanuma et al. [16–21] have calculated IMFPs for 50–2000 eV electrons in over 60 materials (including elements, inorganic compounds, and organic compounds). These calculations were made using an algorithm due to Penn [29] in which the dependence of the inelastic scattering probability on energy transfer was obtained from experimental optical data and the dependence of the scattering probability on momentum transfer was obtained from theory. The latter procedure was necessary because of the lack of relevant experimental data. For each material, checks were made of the optical data using two very useful sum rules [30].

Fig. 1 shows IMFPs for five elements that were calculated from the optical data for each solid. The calculated IMFPs for four of the elements (Al, Cu, Ag, and Au) are of similar magnitudes for electron energies greater than 200 eV. The IMFP for the other element (K) which has the smallest density, however, is about three to four times greater than the corresponding IMFP for the element with the largest density (Au) at energies greater than 200 eV. For electron energies less than 200 eV, the behavior of the IMFP-versus-energy curves is more complicated, the minimum in each curve appearing at substantially different energies. These results are expected from the different electron energy-loss functions for each of these solids [8,9]. The IMFPs shown in Fig. 1 for energies less than 50 eV are given only to indicate trends because the Penn algorithm is not considered reliable in this range [19, 29] but they suggest that the IMFPs for Au are now larger than for the other four elements.

The calculated IMFPs for each material [16–21] were fitted by a modified form of the Bethe [31] equation for inelastic-electron scattering in matter:

$$\lambda = E/\{E_p^2[\beta \ln(\gamma E) - (C/E) + (D/E^2)]\} \quad (2)$$

In Eq. (2), λ is the IMFP (in Å), E is the electron energy (in eV), $E_p = 28.8\ (N_v\ \rho\ /\ M)^{1/2}$ is the free-electron plasmon energy (in eV), ρ is the density (in g cm^{-3}), N_v is the number of valence electrons per atom (for elements) or molecule (for compounds), and M is the atomic or molecular weight. The terms β, γ, C, and D in Eq. (2) are regarded simply as adjustable parameters in the fits to the calculated IMFPs. The modified form of the Bethe equation (that is, the addition of other terms) was suggested by Inokuti [32] and Ashley [33] and was needed to describe the IMFP dependence on energy for energies less than 200 eV [17].

Values of β, γ, C, and D derived from the fits to the calculated IMFPs for 27 elements and 14 organic compounds were analyzed to yield the following expressions in terms of material parameters [20]:

$$\beta = -0.10 + 0.944/(E_p^2 + E_g^2)^{1/2} + 0.069\rho^{0.1} \quad (3a)$$

$$\gamma = 0.191\rho^{-0.50} \quad (3b)$$

$$C = 1.97 - 0.91U \quad (3c)$$

$$D = 53.4 - 20.8U \quad (3d)$$

$$U = N_v\rho/M = E_p^2/829.4 \quad (3e)$$

where E_g is the bandgap energy (in eV) for nonconductors. We note here that IMFPs for a group of 15 inorganic compounds were excluded from this analysis because the optical data for about half of these compounds were judged to be of lower overall

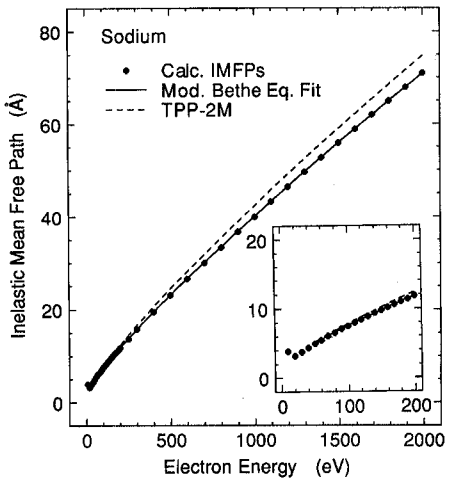

Fig. 2. IMFP values (solid circles) calculated for sodium as a function of electron energy [34]. IMFP values are shown for 10–40 eV electrons to illustrate trends but these results are not considered reliable because the Penn algorithm [29] is not valid for such low energies [16–21]. The solid line is a fit to the IMFP values with the modified Bethe equation (Eq. (2)) and β,γ, C and D are parameters. The dashed line shows IMFP values calculated from the predictive formula TPP-2M (Eqs. (2) and (3a–e)) where values of the four parameters were calculated from property data for sodium using Eqs. (3a–e). The inset shows the low-energy region on an expanded energy scale.

accuracy (and the resulting IMFPs to be less reliable) than for the groups of elements and organic compounds [18]. If appropriate values of material constants are used in Eqs. (3a–e), the average root-mean-square (RMS) deviations of the IMFPs calculated with Eq. (2) from the values calculated directly from optical data were found to be 10.2% for the group of 27 elements, 8.5% for the group of 14 organic compounds, and 18.9% for the group of inorganic compounds. These deviations were considered acceptably small taking into account the empirical nature of Eqs. (3a–e) and the sum-rule errors of the optical data [20]. Eqs. (2) and (3a–e) provide a convenient means to estimate IMFPs for materials other than those for which direct IMFP calculations have been made. These relations have been referred to collectively as the TPP-2M equation [20].

As an example, Fig. 2 shows IMFPs for sodium that were calculated from optical data as described above [34]. The solid points in Fig. 2 are the calculated IMFPs and the solid line is a fit to these data with the modified Bethe equation (Eq. (2)). The dashed line shows IMFPs determined from TPP-2M (Eqs. (2) and (3a–e)). In this case, the RMS deviation between the latter values and the IMFPs from the optical data was found to be 4.9% over the 50–2000 eV energy range. From this and other published examples [20], it was concluded that the TPP-2M equation can provide acceptable estimates of IMFPs for bulk solids. We note here that surface excitations are expected to be important for electron energies less than about 200 eV, and corrections to IMFP data for bulk solids are to be expected [35,36].

An IMFP database will be issued by NIST in 1999 [37].

3. Calculations of mean escape depths

3.1. XPS

Eq. (1) can be used to calculate an MED Δ from an IMFP λ and an electron emission angle α if elastic-electron scattering is neglected. In general, elastic scattering cannot be neglected [13–15], and it is then necessary to calculate the MED D as follows:

$$D = \int_0^\infty z\phi)\mathrm{d}z \Big/ \int_0^\infty \phi(z,\alpha)\mathrm{d}z \tag{4}$$

where $\phi(z,\alpha)$ is the emission depth distribution function (DDF) defined in the Appendix. Calculation of D with Eq. (4) is appropriate because the DDF in AES and XPS can be nonexponential. If elastic-scattering effects were negligible, however, the DDF would be exponential and Eq. (1) could be used to determine the MED.

A formalism has been developed to determine the MED D for signal photoelectrons from amorphous and polycrystalline elemental solids [22–24], and the following analytic formula was derived [24]:

$$D = \lambda\lambda_{tr}[\cos\alpha + (S_1/S_2)]/(\lambda + \lambda_{tr}) \tag{5a}$$

$$\lambda_{tr} = \left[N\int_{4\pi}(1-\cos\xi)(\mathrm{d}\sigma/\mathrm{d}\Omega)\mathrm{d}\Omega\right]^{-1} \tag{5b}$$

$$S_1 \approx (1-\omega)^{-1/2}\chi \tag{5c}$$

$$S_2 \approx (1-\omega)^{-1/2} + (4\pi W(\psi,\beta) - 1)/H(\cos\alpha,\omega) \tag{5d}$$

$$\omega = \lambda/(\lambda + \lambda_{tr}) \tag{5e}$$

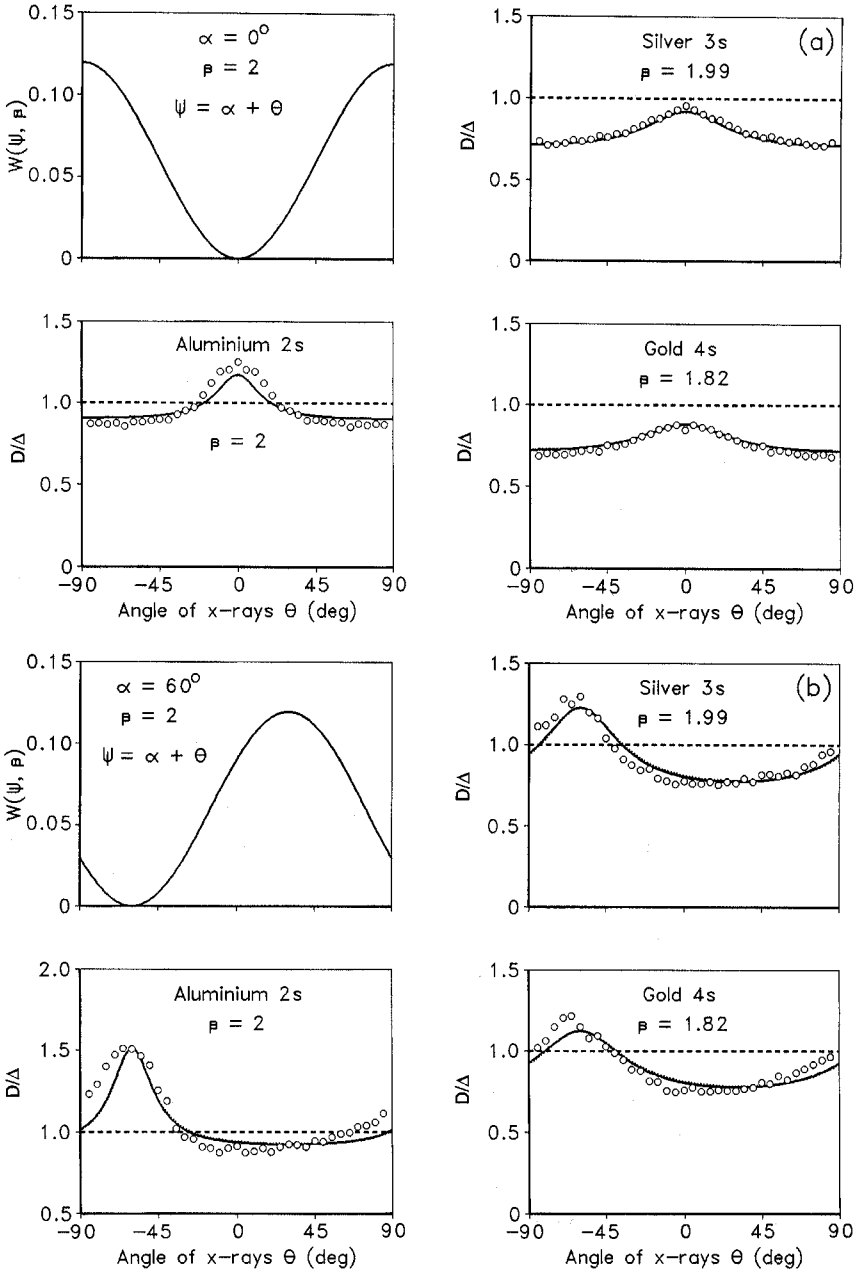

Fig. 3. Comparison of the normalized photoelectric cross sections $W(\psi,\beta)$ with MED results calculated from Eqs. (5a–h) (solid lines) and from Monte Carlo simulations using Eq. (4) (open circles) as a function of the angle of X-ray incidence θ for XPS of the Al 2s, Ag 3s and Au 4s photoelectron lines excited by Mg Kα X-rays [24]. The MED values are shown as the ratio of D from Eq. (4) or (5a–h) to Δ from Eq. (1). The horizontal dashed lines show unity and indicate the result obtained if elastic-electron scattering is neglected. (a) Emission angle $\alpha = 0°$, (b) $\alpha = 60°$ and (c) $\alpha = 80°$.

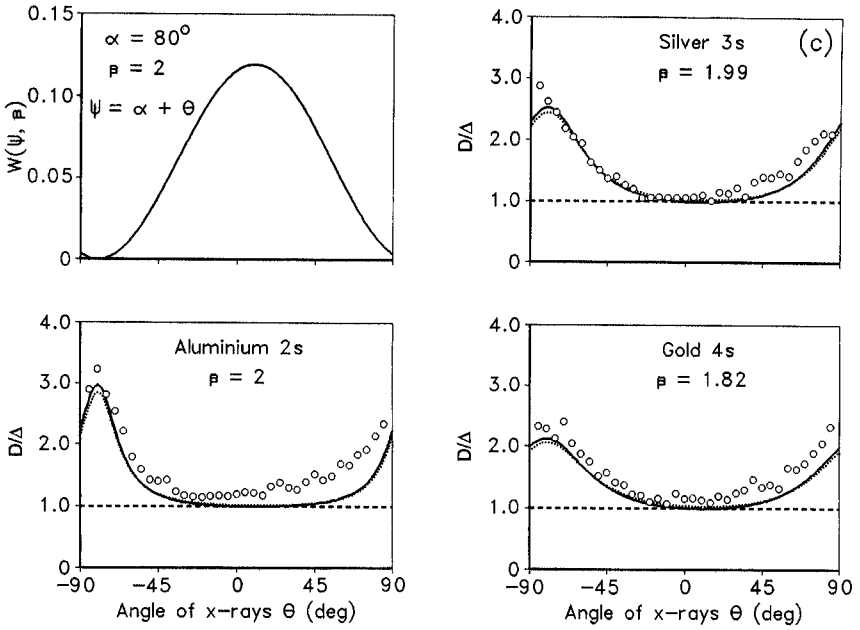

Fig. 3. (*continued*)

$$\chi = (\omega/2)(1-\omega)^{-1/2}\int_0^1 \mu H(\mu,\omega)d\mu \tag{5f}$$

$$W(\psi,\beta) = \left[1 - (\beta/4)\left(3\cos^2\psi - 1\right)\right]/4\pi \tag{5g}$$

$$H(\mu,\omega) \approx (1 + 1.908\mu)/\left[1 + 1.908\mu(1-\omega)^{0.5}\right] \tag{5h}$$

In Eqs. (5a–h)), N is the density of atoms in the elemental solid, λ_{tr} is the transport mean free path (TMFP), $d\sigma/d\Omega$ is the differential elastic-electron scattering cross section, ξ is the polar elastic-scattering angle, β is the asymmetry parameter describing the anisotropy of photoemission, ψ is the angle between the direction of the X-rays and the direction towards the electron energy analyzer, $\mu = \cos\alpha$, $H(\mu,omega;)$ is the H function of Chandrasekhar [38] for an isotropic scattering medium, and Eq. (5h) is an approximation to this function (with a maximum deviation of 3%) proposed by Tilinin and Werner [39]. The ''approximately equals'' signs in Eqs. (5c) and (5d) represent the result of simplifications which lead to errors in D of less than 4% for emission angles smaller than 60°, as judged by XPS calculations for the Al 2s, Al 2p, Ag 3s, Ag 3p, Au 4s, and Au 4p lines with Mg characteristic X-rays and numerous experimental configurations [22–24]; the errors were less than about 8% for larger emission angles. In the formalism leading to Eqs. (5a–h), use was made of the transport approximation [40] in which a realistic differential elastic-scattering cross section was replaced by an isotropic cross section such that the total cross section is given by the transport cross section $(N\lambda_{tr})^{-1}$.

If the electron emission is isotropic, as is expected for AES from amorphous or polycrystalline solids, then $\beta = 0$ in Eq. (5g), and the MED can be determined from the simple formula:

$$D = \lambda\lambda_{tr}(\lambda + \lambda_{tr})^{-1}(\chi + \cos\alpha) \tag{6}$$

If the emission angle α is sufficiently large that $\cos\alpha \ll \chi$, then $D = \lambda\lambda_{tr}\chi/(\lambda + \lambda_{tr})$. However, if the effects of elastic scattering are negligible, $\lambda_{tr} \gg 1$, $\chi \approx 0$, and D from Eq. (6) becomes the same as Δ from Eq. (1).

We proceed now to determine MED values for XPS of elemental solids but will later indicate how MEDs can be found for multicomponent solids. The IMFPs

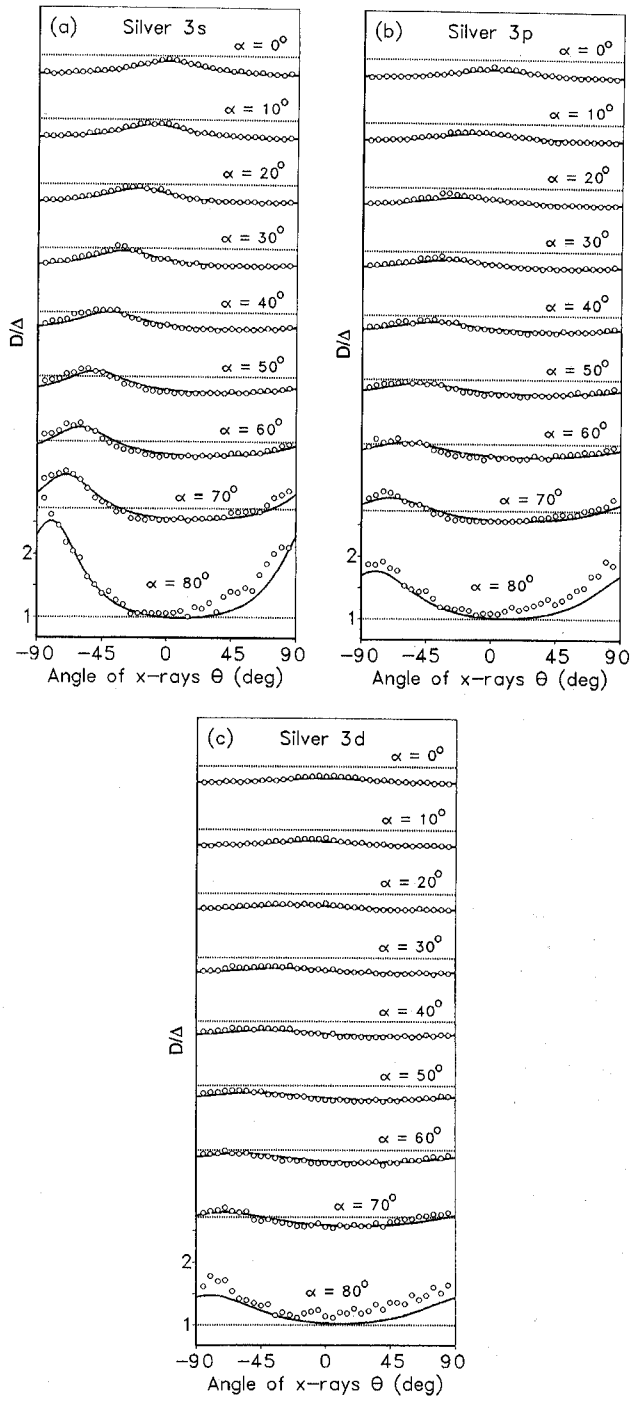

Fig. 4. MED results (shown as the ratio of D from Eq. (4) or (5a–h) to Δ from Eq. (1)) as a function of the angle of X-ray incidence θ for XPS with Mg Kα X-rays from (a) the Ag 3s subshell, (b) the Ag 3p subshell and (c) the Ag 3d subshell [24]. The solid lines show MED results from Eqs. (5a–h) and the open circles represent Monte Carlo simulation data (Eq. (4)). The scale on the ordinate axis refers to the emission angle of 80°. The same scale applies to other emission angles, where the horizontal dotted lines correspond to unity for the plotted ratio.

needed to determine D from Eqs. (5a–h) can be obtained from available data for specific elements [17] or otherwise computed using TPP-2M (Section 2). We note here that tabulations of elemental TMFPs have been published by Jablonski and Tilinin [41] for the most intense photoelectron lines excited by Mg and Al characteristic X-rays; information on TMFP calculations for other photoelectron energies is given below.

We first show comparisons of D values from Eqs. (5a–h) and from Monte Carlo simulations using Eq. (4) [24]. The main value of the Monte Carlo simulations is that structure in the differential elastic-electron-scattering cross sections can be included in the calculations. These simulations, however, are very time consuming. Calculations of D from Eqs. (5a–h) are about a factor of 1000 faster. The comparisons presented as examples here were made to check the reliability of the MED values determined from the transport approximation with Eqs. (5a–h) against values from the Monte Carlo simulations. Details of the calculations are presented elsewhere [24], but we emphasize that the same elastic-scattering cross sections and the same values for other needed parameters (e.g., differential photoionization cross sections and IMFPs) were used in both sets of calculations. One important difference in the two types of calculations, however, was that an analyzer acceptance half-cone angle of 10° was used in the Monte Carlo simulations in order to obtain reasonable statistics in an acceptable time; determinations of D from Eqs. (5a–h) were made on the assumption that the analyzer acceptance angle was negligibly small.

Fig. 3 shows comparisons of MED results from Eqs. (5a–h) and from Monte Carlo simulations using Eq. (4) [24]. It is convenient to plot the MED results in the form $D/\Delta = D/(\lambda \cos\alpha)$ since this ratio would be equal to unity if elastic-scattering effects were negligible; deviations of D/Δ from unity in Fig. 3 indicate the significance of photoelectron elastic scattering. In addition, the quantity $(D/\cos\alpha)$ would be the same as the EAL (see Appendix) in situations where the DDF has at least an approximately exponential variation with depth. Fig. 3 shows MED values for photoelectrons from s subshells (for which the effects of photoemission anisotropy are largest) for three elements (Al, Ag, and Au) covering a wide range of atomic numbers (and thus a wide range of elastic-scattering cross sections). MED values are plotted as a function of angle of X-ray incidence θ (with respect to the surface normal) and for three photoelectron emission angles (0°, 60°, and 80°). For simplicity, the X-ray incidence direction and the photoelectron emission direction have been assumed to be in the same plane normal to the surface; we also note that negative values of θ correspond to the X-ray and analyzer directions being on the same side of the surface normal. In all cases, MED values from Eqs. (5a–h) (shown as the solid lines in Fig. 3) are in generally very good agreement with the corresponding values from Monte Carlo simulations (shown as open circles).

The upper left panels in Figs. 3(a–c) show the function $W(\psi,\beta)$ which specifies the angular anisotropy in the photoemission process (Eq. 5(g)). It can be seen that maxima in the MED plots occur at values of θ corresponding to minima in $W(\psi,\beta)$ and vice versa. The maxima in the MED values for a given emission angle occur when the X-ray direction is close to the analyzer direction. Such XPS configurations are not common in practice although some measurements have been reported using thin films where the analyzer axis has been close to the X-ray direction [42–44]. For high asymmetry of photoemission (e.g., emission from s shells), photoelectrons originating from atoms close to the surface will have a very low probability of entering the analyzer when its axis is close to the surface normal and $\theta = 0°$. Some of these photoelectrons can enter the analyzer but only after one or more elastic collisions. Thus the recorded signal will originate deeper, on the average, than for other configurations, and the MED is correspondingly larger.

Figs. 3(a–c) also show that the ratio D/Δ may exceed unity for certain experimental configurations. At glancing emission angles ($\alpha = 80°$), D/Δ is larger than unity for all values of θ (Fig. 3(c)). The ratio D/Δ is larger than unity when $\alpha = 60°$ for θ between $-85°$ and $-45°$ (Fig. 3(b)). These results are in contrast to the common expectation that the EAL is always smaller than the IMFP. Similar results have been reported previously [14,45].

Fig. 4 shows MED results for XPS from three subshells of silver with Mg Kα X-rays [24]. These MED results are shown as plots of D/Δ as a function of angle of X-ray incidence, as in Fig. 3, for nine

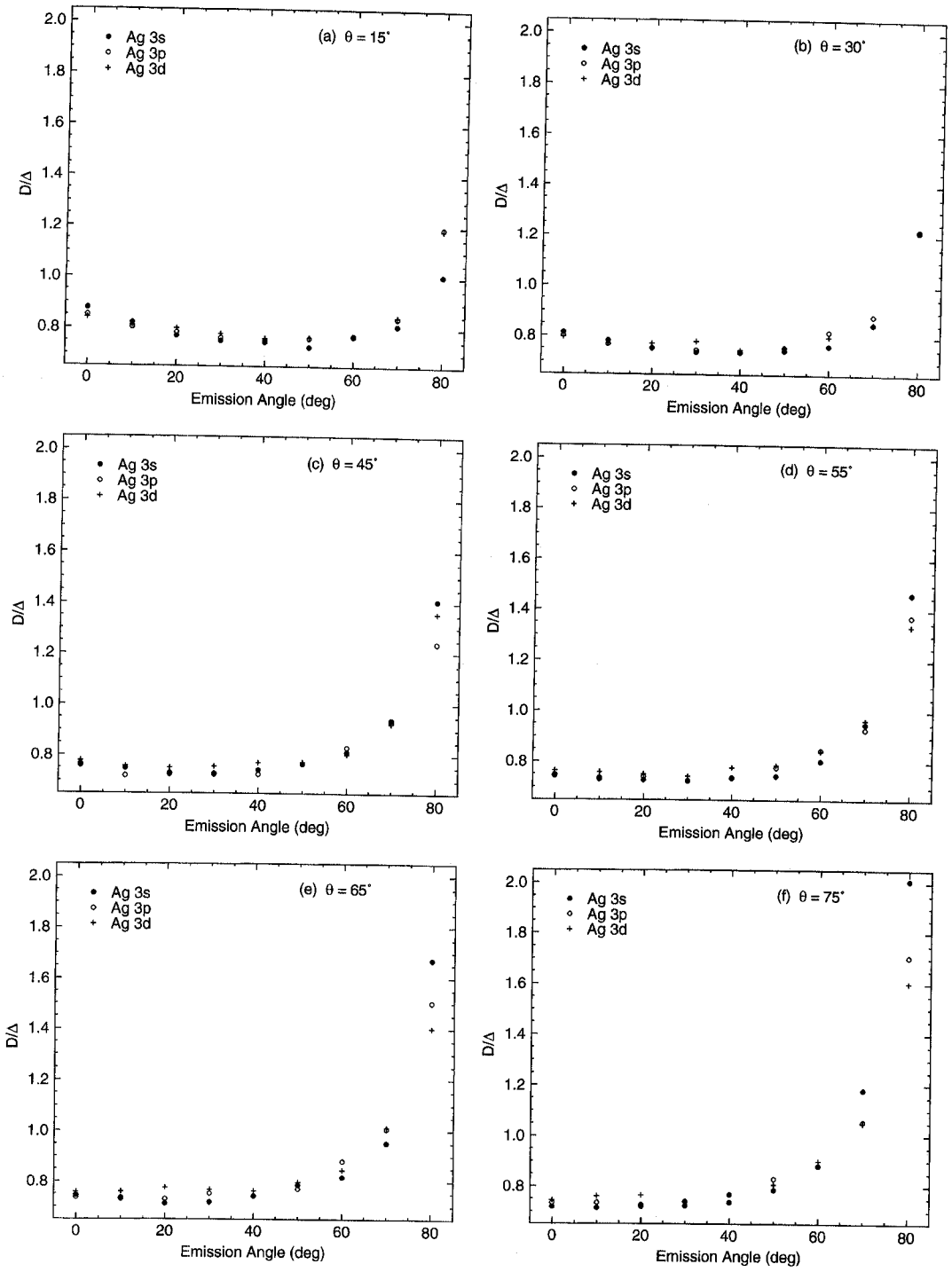

Fig. 5. MED results (shown as the ratio of D from Monte Carlo simulations using Eq. (4) to Δ from Eq. (1)) as a function of photoelectron emission angle for XPS with Mg Kα X-rays from the Ag 3s subshell (●), the Ag 3p subshell (○) and the Ag 3d subshell (+). (a) angle of X-ray incidence $\theta = 15°$, (b) $\theta = 30°$, (c) $\theta = 45°$, (d) $\theta = 55°$, (e) $\theta = 65°$ and (f) $\theta = 75°$.

photoelectron emission angles. The plots were made to show changes in the MED for photoemission from the 3s, 3p, and 3d subshells for which the asymmetry parameter β is 1.99, 1.56, and 1.21, respectively. As expected, the range of D/Δ values for the various emission angles is less for the Ag 3d subshell (which has the the smallest anisotropy) than for the Ag 3p subshell which has a smaller range of D/Δ values than for the Ag 3s subshell. Despite the simplifications introduced by use of the transport approximation in deriving Eqs. (5a–h) [22–24], good agreement is again found between the MED results from Eqs. (5a–h) and the Monte Carlo simulations except when $\alpha = 80°$. The agreement is typically better than about 3% for common XPS conditions ($\theta \leq \pm 45°$ and $\alpha \leq 70°$). For $\alpha = 80°$, however, larger deviations are found.

Fig. 5 shows MED results from the Monte Carlo simulations of Fig. 4 that have now been plotted as a function of photoelectron emission angle α. The D/Δ values are shown for XPS from the same three Ag subshells and for six different angles of X-ray incidence θ. These values of θ were selected to correspond to those that are common or might be selected in many XPS measurements and particularly for ARXPS. The angle between the X-ray and analyzer directions in commercial XPS instruments is generally constant; in some instruments, this angle is close to the so-called magic angle (54.7°) but can vary between 35° and 90° [46]. We show MED results in Fig. 5(d) for $\theta = 55°$ (close to the magic-angle configuration) and for which photoelectrons can be readily detected at emission angles ranging from 0° to 80°. We also show MED results for three smaller values of θ (15°, 30°, and 45°) in Figs. 5(a–c) and for two larger values of θ (65° and 75°) in Figs. 5(e) and (f) to illustrate the effects of changing θ. We note here that the effects of elastic-electron scattering are now ignored in the algorithms used to obtain composition-versus-depth information from measurements of photoelectron or Auger-electron signals as a function of emission angle [11,12].

The MED results in Fig. 5 show two important results. First, over a range of emission angles of typically 40°–60°, values of D/Δ are approximately constant to within 10% for a given value of θ and for a particular subshell. For $\theta = 55°$, for example, the average value of D/Δ is 0.747 for the Ag 3s subshell and α varying from 0° to 60°, 0.744 for the Ag 3p subshell for α varying from 0° to 50°, and 0.764 for the Ag 3d subshell for α varying from 0° to 50°. Similar but not identical values of this ratio occur for the other values of θ shown in Fig. 5. The particular range of emission angles, however, over which D/Δ is approximately constant varies from about 10° to 70° for the Ag 3s subshell with $\theta = 15°$ to about 0° to 40° for the Ag 3p subshell with $\theta = 75°$. Depending on the particular value of θ and the particular Ag subshell, the average value of D/Δ (calculated over the emission-angle range where this ratio does not change by more than 10%) varies from 0.73 to 0.79. This result is useful because it shows that ARXPS data for Ag could be analyzed with confidence over a now-known range of emission angles where D/Δ is sufficiently constant for most ARXPS applications and where the EAL (given by $D/\cos\alpha$) is here approximately 0.76 of the IMFP for the relevant photoelectrons. The particular value for the EAL (corresponding to the subshell, θ, and the range of emission angles being analyzed) could then be used to establish the depth scale in the derived composition–depth profile.

The second main result from Fig. 5 is that the values of D/Δ increase substantially for the more grazing emission angles. For example, D/Δ for $\alpha = 80°$ can be twice or more the values found for emission angles between 0° and 60°. This result shows very clearly that the improvement in surface sensitivity (a smaller value of D) from acquiring XPS data at $\alpha = 80°$ would be much less than expected from a naive use of Eq. (1) (which is based on neglect of the effects of elastic-electron scattering). A similar conclusion is obtained from the D/Δ values shown in Fig. 3(c) for XPS from the Al 2s and Au 4s subshells.

It is recommended that those applying ARXPS make use of Eqs. (5a–h) to determine the emission angle range over which D/Δ is approximately constant (for a particular element, photoelectron line, and value of θ). This angular range should not be exceeded in the ARXPS experiments. The calculated EAL value for this angular range can then be used (as the ''lambda value'') to determine the depth scale in the analysis of the ARXPS data.

We consider now MED values for multicomponent solids (e.g., compounds and alloys). Eqs. (5a–h) can be used for this purpose except that TMFP values

should be computed from

$$\lambda_{tr} = \left[N_0 \sum_{j=1}^{n} \left(x_j / N_j \lambda_{tr,j} \right) \right]^{-1} \quad (7)$$

rather than Eq. (5b). In Eq. (7), n is the number of elements in the solid, N_0 is the atomic density of the solid, N_j is the atomic density of the jth element in its pure form, and x_j is the atom fraction of the jth element. If the solid contains elements that are normally gaseous (e.g., oxides or chlorides), the value of λ_{tr} can be expressed in terms of the transport cross sections $\sigma_{tr,j}$ for the elemental constituents [47]:

$$\lambda_{tr} = (N_0 \sigma_{tr})^{-1} \quad (8a)$$

where

$$\sigma_{tr} = \sum_{j=1}^{n} x_j \sigma_{tr,j} \quad (8b)$$

Values of $\sigma_{tr,j}$ can be estimated from the quasi-classical expression of Tilinin [48,49], taken from published tables [50], or calculated from the defining formula:

$$\sigma_{tr} = \int_{4\pi} \frac{d\sigma}{d\Omega} (1 - \cos\xi) d\Omega$$

$$= 2\pi \int_0^{\pi} \frac{d\sigma}{d\Omega} (1 - \cos\xi) \sin\xi d\xi \quad (8c)$$

where $d\sigma/d\Omega$ is the differential elastic-electron scattering cross section for polar scattering angle ξ. Differential cross sections for all elements and for electron energies between 50 and 10,000 eV are available in a database [51].

Cumpson and Seah [52] have recently reported calculations of EALs in 27 elements based on the IMFP results of Tanuma et al. [17]. These authors performed Monte Carlo simulations of electron transport for overlayer films of varying thickness on a substrate of the same element and for various emission angles. From an analysis of their EAL values, Cumpson and Seah derived two formulae (for 100–2000 eV electrons and a specified range of emission angles) which can be used to calculate EAL values and thus to derive overlayer film thicknesses in AES and XPS experiments. We point out here two limitations of this analysis which are only briefly noted in their paper [52]. First, it is expected that there will be different EAL values for overlayer and substrate materials with substantially different atomic numbers (as a result of their different elastic-scattering properties), as found previously by Jablonski and Tougaard [53]. Second, no account was taken in the simulations of the effects of photoionization anisotropy which is known to be important in XPS (as discussed here and elsewhere [13–15,54,55]). It is therefore recommended that the results and formulae of Cumpson and Seah not be used for EAL calculations in XPS until the effect of photoionization anisotropy on their derived EAL values has been examined. We also point out that the Cumpson–Seah formulae were derived from data for elemental solids and their reliability for determining thicknesses of compounds (e.g., oxides) on elemental or other substrates has not yet been evaluated.

Zemek et al. [56] have measured MEDs from the intensities of O 1s photoelectrons (with a kinetic energy of 956 eV) and Al 2s photoelectrons (with an energy of 1368 eV) excited by Al Kα X-rays in thin layers of Al_2O_3 on Al. The intensities were measured as a function of oxide thickness for photoelelectron emission angles ranging from 0° to 60°. Although the effects of elastic-electron scattering are weak in O and Al (because of their low atomic numbers), ratios of measured MED values for $\alpha = 0°$ and $\alpha = 60°$ were about 2.7 while the calculated ratios assuming neglible elastic scattering were 2.0. The MEDs measured by Zemek et al. were also found to be in good agreement with values calculated from Monte Carlo simulations and from Eqs. (5a–h). The elastic-scattering effects are expected to be larger for heavier elements.

Tilinin [23] has derived an analytic formula which can be used to obtain MED values for photoelectrons emitted from solids by polarized X-rays (which can be frequently encountered in XPS experiments with synchrotron radiation). The ratio D/Δ can vary substantially, between 0.7 and 2.9 for photoemission from the Al 2s and Au 4s subshells by 1486.5 eV X-rays, depending on the X-ray polarization and the photoelectron emission direction.

3.2. AES

We consider now EAL and MED values for Auger

electrons emerging from elemental solids. As for XPS, IMFPs can be estimated using TPP-2M (Section 2).

Jablonski [25–28] has reported the results of many Monte Carlo simulations of Auger-electron intensities that would be measured by a cylindrical-mirror analyzer (CMA) with its axis normal to the specimen surface. He found that the DDFs from the simulations for many elements and matrices were close to exponential with depth. The resulting values of the EAL, λ_{EAL}, could then be related to the corresponding IMFPs by the simple relation:

$$k = \lambda_{EAL}/\lambda \quad (9)$$

Values of k fell in the following ranges for the KLL, L_3MM, and M_5NN Auger series: (a) from 0.882 to 0.926 for the most pronounced KLL Auger transitions of C, Al, and Si (with energies from 272 to 1619 eV); (b) from 0.700 to 0.868 for the most pronounced L_3MM transitions for Al, Si, Cr, Fe, Ni, Cu, Ge, Zr, Nb, and Mo (with energies from 68 to 2044 eV); and (c) from 0.664 to 0.794 for the most pronounced M_5NN Auger transitions in Zr, Nb, Mo, Pd, Ag, La, Gd, Ta, W, Pt, and Au[25]. Values of k were slightly smaller for the boron KLL Auger transition in a number of matrices [26]. For these analytical situations, the MED is simply given by:

$$D = \lambda_{EAL}\cos\alpha \quad (10)$$

For a CMA with its axis normal to the specimen surface, the average value of α is 42.3°, and D is then simply $0.74\lambda_{EAL}$. If, for illustrative purposes, we use an average value of $k = 0.8$ [25], D would then be 0.59λ.

We also note that the value of $k = 0.709$ found by Jablonski [25] for a CMA measurement of the Ag M_5VV Auger transition at 356 eV is very close to the corresponding values of D/Δ (≈ 0.75) for XPS from the Ag 3s subshell at a somewhat larger photoelectron kinetic energy (536 eV) and for non-grazing emission angles in Fig. 5.

Ding and Shimizu [57] performed Monte Carlo simulations to determine MEDs for a CMA with its axis tilted at varying angles to the surface normal. For zero tilt angle, these authors found values of D ranging from 0.47λ to 0.57λ for the Cu MVV Auger transition at 59 eV and the Au NVV transition at 238 eV, respectively; D values for the Cu L_3VV Auger transition at 916 eV and the Au N_4VV transition at 2025 eV were close to the value for the 238 eV Au transition. As the CMA axis was tilted up to 60°, the D values changed very little; for larger tilt angles, unlikely to be used in practical AES, the D values decreased to $0.41\ \lambda$ and 0.46λ for the 59 eV Cu and 238 eV Au transitions, respectively.

For a hemispherical analyzer, values of D can be simply calculated from Eq. (6) for the particular element, Auger-electron energy, and emission angle.

4. Summary

We have presented an overview of methods to determine the surface sensitivity in XPS and AES. A basic parameter is the inelastic mean free path (IMFP) for bulk solids. IMFPs have been calculated for many elemental solids, inorganic compounds, and organic compounds, and the predictive IMFP formula TPP-2M (Eqs. (2) and (3a–e)) can be used to estimate IMFPs for other materials [20]. The so-called "universal curve" [10] is generally not a reliable guide to IMFP magnitudes or to the dependence of IMFP on electron energy. Formulae based on early measurements of effective attenuation lengths [5] are similarly expected to be useful only as semi-quantitative guides because of substantial uncertainties concerning the morphology and structure of the films used in the early experiments.

If elastic-electron scattering is neglected, the depth distribution function (DDF) of the signal electrons will be exponential with depth and the exponential parameter will be the IMFP. The effective attenuation length (EAL) will then be equal to the IMFP and the mean escape depth (MED) will be the product of the IMFP and the cosine of the emission angle (Eq. (1)).

We have examined the elastic-scattering effects in AES and XPS using atomic elastic-scattering cross sections and expect the results to be applicable to amorphous and polycrystalline solids. We find that the effects of elastic scattering are usually not negligible, and that the DDF is often not exponential with depth. For some analytical situations (e.g., AES with a cylindrical-mirror analyzer (CMA)), the DDF is approximately exponential and the exponential parameter will be the EAL. The EAL can be up to about 35% smaller than the IMFP. Since the average

emission angle for a CMA with its axis normal to the specimen surface is 42.3°, the MED for AES measurements will be 0.74 times the EAL (Eqs. (8a–c)). If, for example, the ratio of the EAL to the IMFP is 0.8, the MED will be 0.59 times the IMFP. This example illustrates the magnitude of the numerical differences that can arise among the IMFP, EAL, and MED. These three terms are not only conceptually different (see Appendix) but can have different magnitudes that can be important in practical applications.

For XPS, the situation is more complicated than for AES on account of the angular anisotropy in the photoemission process. The DDF is generally not exponential with depth, and it is then appropriate to use the MED as a measure of the surface sensitivity. MEDs can be determined analytically using Eqs. (5a–h) for elemental solids with calculated or estimated IMFPs, values of the transport mean free path (determined from atomic elastic-electron scattering cross sections), and information on the experimental configuration (angle of X-ray incidence and photoelectron emission angle) [22-24]. Comparisons have been made here between MEDs from Eqs. (5–h) and values obtained from Monte Carlo simulations for XPS with Mg Kα X-rays. These comparisons were made for photoelectrons from the Al 2s, Ag 3s, Ag 3p, Ag 3d, and Au 4s subshells and a wide variety of possible instrumental configurations. In general, the agreement between the two sources of MED data was very good. Since MEDs can be computed much more rapidly and easily with the analytic formalism than by Monte Carlo simulations, the former approach can be readily used to provide MEDs for different possible XPS experiments. The MED values found here for near-normal emission angles are up to about 30% *less* than the values found from Eq. (1) (for which elastic-scattering effects were neglected). In addition, MEDs can be much *larger* (by up to about a factor of two) than expected from Eq. (1) for near-grazing emission angles or for certain other instrumental configurations. For common XPS measurement conditions, MEDs can deviate substantially (typically by $\pm$30%) from the results of Eq. (1). It is therefore possible for photoelectrons and Auger electrons of the same energy from some material to have different MEDs.

ARXPS is now commonly used to obtain composition–depth information but elastic-scattering effects are ignored in present data-analysis algorithms [11,12]. We have shown that there is a limited range of photoelectron emission angles over which the ratio of MEDs from Eqs. (5a–h) and Eq. (1) does not change by more than 10%. This angular range was found to be between 40° and 60° for the case of photoemission with Mg Kα X-rays from three silver subshells considered here. In general, ARXPS experiments should be performed over a sufficiently limited range of emission angles to minimize artifacts caused by the neglect of elastic-electron scattering. MEDs can be computed from Eqs. (5a–h) for the element and subshell of interest, the angle of X-ray incidence, and the experimentally accessible range of emission angles to find the emission-angle range for ARXPS over which the ratios of the MED to the results from Eq. (1) are sufficiently constant. This ratio also provides an EAL for use in the analysis of the ARXPS data, thereby establishing the experimental depth scale.

Finally, we point out that the ratio of the MED for an emission angle of 80° in XPS to the value found from Eq. (1) can be twice or more the value found for emission angles between 0° and 60°. It is therefore clear that any improvement in surface sensitivity from use of the near-grazing emission angle would be much less than that expected from a simplistic use of Eq. (1).

Acknowledgements

One of the authors (A.J.) wishes to acknowledge support under KBN Grant No. 2PO3B 009 10.

Appendix A. Definition of terms

The following definitions of terms relating to surface sensitivity were developed by ASTM Committee E-42 on Surface Analysis [58].

Inelastic mean free path: the average of distances, measured along the trajectories, that particles with a given energy travel between inelastic collisions in a substance.

Emission depth distribution function (for a measured signal): for particles or radiation emitted from a surface in a given direction, the probability that the

particle or radiation leaving the surface in a specified state originated from a specified depth measured normally from the surface into the material.

Average emission function decay length: the negative reciprocal slope of the logarithm of a specified exponential approximation to the emission depth distribution function over a specified range of depths, as determined by a straight-line fit to the emission depth distribution function plotted on a logarithmic scale versus depth on a linear scale.

Effective attenuation length: the average emission function decay length when the emission depth distribution function is sufficiently close to exponential for a given application.

Mean escape depth: the average depth normal to the surface from which the specified particles or radiation escape as defined by: $\int_0^\infty z\phi(z,\alpha)\mathrm{d}z / \int_0^\infty \phi(z,\alpha)\mathrm{d}z$, where $\phi(z,\alpha)$ = the emission depth distribution function for depth z from the surface into the material and for direction of emission α with respect to the surface normal.

Information depth: maximum depth, normal to the specimen surface, from which useful signal information is obtained.

Note 1. The information depth can be identified with the specimen thickness from which a specified percentage (e.g., 95% or 99%) of the detected signal originates.

Note 2. The information depth can be determined from a measured, calculated, or estimated depth distribution function for the signal of interest.

References

[1] S. Hofmann, Surf. Interface Anal. 9 (1986) 3.
[2] C.R. Brundle, J. Vac. Sci. Technol. 11 (1974) 212.
[3] C.J. Powell, Surf. Science 44 (1974) 29.
[4] I. Lindau, W.E. Spicer, J. Electron Spectrosc. Relat. Phen. 3 (1974) 409.
[5] M.P. Seah, W.A. Dench, Surf. Interface Anal. 1 (1979) 2.
[6] C.J. Powell, J. Electron Spectrosc. Relat. Phen. 47 (1988) 197.
[7] C.J. Powell, M.P. Seah, J. Vac. Sci. Technol. A8 (1990) 735.
[8] S. Tanuma, C.J. Powell, D.R. Penn, J. Electron Spectrosc. Relat. Phenom. 52 (1990) 285.
[9] S. Tanuma, C.J. Powell, D.R. Penn, J. Vac. Sci. Technol. A8 (1990) 2213.
[10] G.A. Somorjai, Introduction to Surface Chemistry and Catalysis, Wiley, New York, 1994.
[11] B.J. Tielsch, J.E. Fulghum, Surf. Interface Anal. 21 (1994) 621.
[12] P.J. Cumpson, J. Electron Spectrosc. Relat. Phenom. 73 (1995) 25.
[13] A. Jablonski, Surf. Science 188 (1987) 164.
[14] A. Jablonski, H. Ebel, Surf. Interface Anal. 11 (1988) 627.
[15] A. Jablonski, Surf. Interface Anal. 15 (1990) 559.
[16] S. Tanuma, C.J. Powell, D.R. Penn, Surf. Interface Anal. 11 (1988) 577.
[17] S. Tanuma, C.J. Powell, D.R. Penn, Surf. Interface Anal. 17 (1991) 911.
[18] S. Tanuma, C.J. Powell, D.R. Penn, Surf. Interface Anal. 17 (1991) 929.
[19] S. Tanuma, C.J. Powell, D.R. Penn, Surf. Interface Anal. 20 (1993) 77.
[20] S. Tanuma, C.J. Powell, D.R. Penn, Surf. Interface Anal. 21 (1994) 165.
[21] S. Tanuma, C.J. Powell, D.R. Penn, Surf. Interface Anal. 25 (1997) 25.
[22] I.S. Tilinin, A. Jablonski, B. Lesiak-Orlowska, Acta Phys. Polonica A86 (1994) 845.
[23] I.S. Tilinin, Phys. Rev. B 53 (1996) 547.
[24] A. Jablonski, I.S. Tilinin, C.J. Powell, Phys. Rev. B 54 (1996) 10927.
[25] A. Jablonski, Surf. Science 188 (1987) 164.
[26] A. Jablonski, M. Krawczyk, B. Lesiak, J. Electron Spectrosc. Relat. Phenom. 46 (1988) 131.
[27] A. Jablonski, Surf. Interface Anal. 14 (1989) 659.
[28] A. Jablonski, Surf. Interface Anal. 15 (1990) 559.
[29] D.R. Penn, Phys. Rev. B 35 (1987) 482.
[30] S. Tanuma, C.J. Powell, D.R. Penn, J. Electron Spectrosc. Relat. Phenom. 62 (1993) 95.
[31] H. Bethe, Ann. Physik 5 (1930) 325.
[32] M. Inokuti, Rev. Mod. Phys. 43 (1971) 297.
[33] J.C. Ashley, J. Electron Spectrosc. Relat. Phen. 46 (1988) 199.
[34] S. Tanuma, C.J. Powell, D.R. Penn (to be published).
[35] F. Yubero, S. Tougaard, Phys. Rev. B 46 (1992) 2486.
[36] Y.F. Chen, J. Vac. Sci. Tech. A13 (1995) 2665.
[37] NIST Electron Inelastic-Mean-Free-Path Database, Standard Reference Data Program Database 71 (National Institute of Standards and Technology, Gaithersburg, MD, 1999).
[38] S. Chandrasekhar, Radiative Transfer (Clarendon, Oxford, 1950), p. 6.
[39] I.S. Tilinin, W.S.M. Werner, Surf. Science 290 (1993) 119.
[40] I.S. Tilinin, W.S.M. Werner, Phys. Rev. B 46 (1992) 13739.
[41] A. Jablonski, I.S. Tilinin, J. Electron Spectrosc. Relat. Phenom. 74 (1995) 207.
[42] O.A. Baschenko, G.V. Machavariani, V.I. Nefedov, J. Electron Spectrosc. Relat. Phenom. 34 (1984) 305.
[43] A. Jablonski, J. Zemek, Phys. Rev. B 48 (1993) 4799.
[44] A. Jablonski, J. Zemek, Surf. Science 387 (1997) 288.
[45] A. Jablonski, Surf. Interface Anal. 21 (1994) 758.
[46] M.P. Seah, Surf. Interface Anal. 20 (1993) 243.
[47] I.S. Tilinin, A. Jablonski, B. Lesiak, Appl. Surf. Science 100/101 (1996) 20.
[48] I.S. Tilinin, Sov. Phys. JETP, 67 (1988) 1570 (Zh. Eksp. Teor. Fiz. 94 (1988) 96).

[49] I.S. Tilinin, Phys. Rev. A 51 (1995) 3058.
[50] R. Mayol, F. Salvat, Atomic Data and Nuclear Data Tables, 65 (1997) 55.
[51] NIST Elastic-Electron-Scattering Cross-Section Database, Standard Reference Data Program Database 64 (National Institute of Standards and Technology, Gaithersburg, MD, 1996).
[52] P.J. Cumpson, M.P. Seah, Surf. Interface Anal. 25 (1997) 430.
[53] A. Jablonski, S. Tougaard, J. Vac. Sci. Tech. A8 (1990) 106.
[54] A. Jablonski, C.J. Powell, Phys. Rev. B 50 (1994) 4739.
[55] A. Jablonski, C.J. Powell, J. Vac. Sci. Tech. A15 (1997) 2095.
[56] J. Zemek, S. Hucek, A. Jablonski, I.S. Tilinin, J. Electron Spectrosc. Relat. Phenom. 76 (1995) 443.
[57] Z.-J. Ding, R. Shimizu Surf. Interface Anal. 23 (1995) 351.
[58] Standard E 673, Annual Book of ASTM Standards, Vol. 3.06 (American Society for Testing and Materials, West Conshohocken, Pennsylvania, 1998).